J. Am. Soc. Mass Spectrom. (2015) 26:1283–1290
DOI: 10.1007/s13361-015-1159-1

RESEARCH ARTICLE

Argon Cluster Sputtering Source for ToF-SIMS Depth Profiling of Insulating Materials: High Sputter Rate and Accurate Interfacial Information

Zhaoying Wang,[1,2] Bingwen Liu,[2] Evan W. Zhao,[2] Ke Jin,[2] Yingge Du,[3] James J. Neeway,[4] Joseph V. Ryan,[4] Dehong Hu,[2] Kelvin H. L. Zhang,[3] Mina Hong,[2] Solenne Le Guernic,[2] Suntharampilai Thevuthasan,[2] Fuyi Wang,[1] Zihua Zhu[2]

[1]Beijing National Laboratory for Molecular Sciences, CAS Key Laboratory of Analytical Chemistry for Living Biosystems, Beijing Centre for Mass Spectrometry, Institute of Chemistry, Chinese Academy of Sciences, Beijing, 100190, People's Republic of China
[2]W. R. Wiley Environmental Molecular Sciences Laboratory, Pacific Northwest National Laboratory, Richland, WA 99354, USA
[3]Fundamental and Computer Sciences Directorate, Pacific Northwest National Laboratory, Richland, WA 99354, USA
[4]Energy and Environment Directorate, Pacific Northwest National Laboratory, Richland, WA 99354, USA

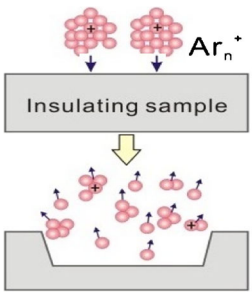

Abstract. The use of an argon cluster ion sputtering source has been demonstrated to perform superiorly relative to traditional oxygen and cesium ion sputtering sources for ToF-SIMS depth profiling of insulating materials. The superior performance has been attributed to effective alleviation of surface charging. A simulated nuclear waste glass (SON68) and layered hole-perovskite oxide thin films were selected as model systems because of their fundamental and practical significance. Our results show that high sputter rates and accurate interfacial information can be achieved simultaneously for argon cluster sputtering, whereas this is not the case for cesium and oxygen sputtering. Therefore, the implementation of an argon cluster sputtering source can significantly improve the analysis efficiency of insulating materials and, thus, can expand its applications to the study of glass corrosion, perovskite oxide thin film characterization, and many other systems of interest.

Keywords: ToF-SIMS, Argon cluster, SON68 glass, Perovskite oxide thin films, Sputtering rate, Charging alleviation

Received: 12 December 2014/Revised: 17 March 2015/Accepted: 1 April 2015/Published Online: 8 May 2015

Introduction

Depth profiling using time-of-flight secondary ion mass spectrometry (ToF-SIMS) has been widely utilized in semiconductor industry for more than 20 years [1]. Recently, it has become increasingly popular in the fields of biology, geology, and novel material research [2]. However, unlike in semiconductor industry, the majority of samples in these new application fields are insulators.

In ToF-SIMS depth profiling analysis, a dual-beam operation composed of a sputtering and an analysis beam is typically used. The analysis beam is optimized for collecting high-quality mass spectra, and the sputtering beam is optimized for high sputter rate, optimum depth resolution, and optimum ionization yield [1]. Two operation modes are generally performed: interlaced mode and non-interlaced mode. In interlaced mode, the beam is active between two analysis shots that are operated quasi-simultaneously. It is commonly applied for depth profiling of conductive or semiconductive samples, having the advantage of time-saving and the ability to provide full depth information [1]. However, for depth profiling of insulating samples, the employment of a low energy (≤10 eV) electron beam is not sufficiently effective to compensate the intensive charge accumulation at the sputtering interface, especially for traditional O_2^+ and Cs^+ sputtering beams (low energy (0.2–

Electronic supplementary material The online version of this article (doi:10.1007/s13361-015-1159-1) contains supplementary material, which is available to authorized users.

Correspondence to: Fuyi Wang; *e-mail:* fuyi.wang@iccas.ac.cn, Zihua Zhu; *e-mail:* zihua.zhu@pnnl.gov

2.0 kV) and high current (tens to hundreds nA)) [3]. To this end, non-interlaced mode is proposed, in which the sputtering phases (typically, several seconds each) and the analysis phases (several seconds each) are separated, and charge compensation time slots (several seconds each) are added in between.

Although the non-interlaced mode can effectively alleviate the charging effect to a limited extent, its measurement is normally 3–5 times longer than the interlaced mode if a similar depth resolution is required, making the deep depth profiling (e.g., 1–10 μm) of insulating samples a time-consuming task [3].

Since argon cluster (Ar_n^+) ion sources were implemented in SIMS [4, 5] and subsequently used in X-ray photoelectron spectroscopy (XPS) [6] and ultraviolet photoelectron spectroscopy (UPS) [7], it has been widely applied for the molecular depth profiling of polymers, biological molecules, and other organic materials because they can retain molecular information during the erosion process. In addition, they can provide high sputtering rate, allowing the fast depth profiling of above soft materials [8–15]. However, the application of Ar_n^+ ion source to depth profiling of inorganic insulating materials has rarely been attempted, possibly because of the lesser efficiency-enhancing ionization yield compared with O_2^+ and Cs^+ ion sources for both positive and negative ions.

In this work, we evaluated the performance of an Ar_n^+ sputtering source in ToF-SIMS compared with traditional O_2^+ and Cs^+ ion sources in terms of efficiency, accurate interfacial chemical information, and mass resolution in depth profiling of several representative insulating samples. A leached simulated borosilicate nuclear waste glass(SON68), a $La_{0.93}Sr_{0.07}CrO_3$ thin film on a $SrTiO_3$ substrate, and a $SrTiO_3/SrCrO_3$ bi-layer film on a $SrTiO_3$ substrate were selected as model systems for our study because of their fundamental and practical importance[16–26].

Experimental

Materials and Sample Preparation

The components, preparation, and leaching procedure of the SON68 glass have been described elsewhere [20, 27]. In brief, it was made by batching carbonates and oxides of the various metals, melting in a furnace, and quenching on a stainless steel plate. This glass was then pulverized and re-melted to ensure a homogeneous solid. The second melt was poured into molds to produce rectangular bars. Coupons (~10 × 10 × 1 mm^3) were cut from the bars and both sides of the coupons were polished. To study the diffusion behavior of Li, the SON68 coupons (natural isotopic abundance for all elements) were submerged in a solution of a dimethyl sulfoxide (DMSO) with dissolved LiCl (^{6}Li enriched, ^{6}Li:^{7}Li = 95:5). The coupons were in contact with the solution at 150°C for 10 d. When the coupons were removed from the vessel, they were rinsed with clean DMSO, water, then ethanol, and dried in an oven.

Epitaxial $La_{0.93}Sr_{0.07}CrO_3$ (in brief, $LaSrCrO_3$) thin films with a thickness of ~66 nm were grown on TiO_2-terminated $SrTiO_3$ (001) substrates by molecular beam epitaxy (MBE). The detailed preparation process has been described elsewhere [26]. In brief, the substrates were loaded into an ultrahigh vacuum chamber and heated at 700°C prior to growth. La, Sr, and Cr were evaporated for high-temperature effusion cells, and flux rates were calibrated using a quartz crystal microbalance (QCM). The O_2 partial pressure was kept at ~2.0×10^{-6} Torr during growth. The procedures for epitaxial growth of $SrTiO_3/SrCrO_3$ on $SrTiO_3$ are essentially the same as those of $La_{0.93}Sr_{0.07}CrO_3$, except that the oxygen line was changed to isotope $^{18}O_2$. A 50 nm thick $SrCrO_3$ film was grown first on TiO_2-terminated $SrTiO_3$, then followed by 50 nm thick $SrTiO_3$.

Depth Profiling

Dual beam depth profiling experiments were performed on a ToF-SIMS instrument (TOF.SIMS5; IONTOF GmbH, Münster, Germany) in the Environmental Molecular Sciences Laboratory (EMSL), located at Pacific Northwest National Laboratory (PNNL). Three sputtering ion sources were available: Ar_n^+ (2.5–20 keV), O_2^+ (0.2–2.0 keV), and Cs^+ (0.2–2.0 keV) sources. A 25 keV pulsed Bi^+ ion beam was used as the analysis beam, and the analysis area was 100 × 100 μm^2 or 50 × 50 μm^2 at the center of the sputter crater. Interlaced mode was applied to most measurements because it is more time-efficient than non-interlaced mode. Non-interlaced mode was applied to compare signal intensity, mass resolution, and also to prove the accuracy of interfacial chemical information. Charge compensation was used for all depth profiling measurements. The details for the adjustment of charge compensation and additional information for ToF-SIMS measurement can be found in our previous publication [28].

The depths and crater shapes of sputter craters were measured using a Dektak 6 M stylus profilometer (UT, USA). For convenience, a constant sputter rate was adopted in each measurement. Tapping mode atomic force microscope (AFM) (Digital Instruments (Veeco) Nanoscope III Multimode, Tonawanda, New York, USA) was used to characterize the roughness of the crater bottoms. The craters in $LaSrCrO_3/SrTiO_3$ thin film were imaged using TESP silicon probes (Veeco probes) (42 N/m nominal stiffness), operating at a set point of 80% of its free amplitude. Both height and phase data were collected simultaneously during the characterization.

Results and Discussion

Sputter Rate

In absolute terms, the sputter rate of the Ar_n^+ source on inorganic materials may not be as good as that of the O_2^+ or Cs^+ sources. For example, on the updated IONTOF instrument (TOF.SIMS5) in EMSL, with a 300 × 300 μm^2 sputtering area, the highest sputter rate of the Ar_n^+ ion source on a SON68 glass sample is about 0.73 nm/s (20 keV Ar_{1500}^+, 12 nA). This is lower than 1.5 nm/s for the O_2^+ source (2.0 keV O_2^+, 600 nA) and 0.82 nm/s for the Cs^+ source (2.0 keV Cs^+, 150 nA)

Table 1. The Highest Sputter Rates of Different Ion Sources Over Different Analysis Areas on a SON68 Glass Sample

Sputter source	Beam energy (keV)	Beam current (nA)	Sputter rate at default sputter size 300 × 300 μm² (nm/s)	Sputter yield (nm³/ion)	Required analysis area (μm²)				
					100 × 100		50 × 50		
					Minimum sputter size (μm)	Maximum sputter rate (nm/s)	Minimum sputter size (μm)	Maximum sputter rate (nm/s)
Ar_n^+	20	12.0	0.73 ± 0.04	0.88 ± 0.08	150	2.90 ± 0.15	100	6.50 ± 0.24
	10	9.0	0.11 ± 0.01	0.18 ± 0.01	150	0.43 ± 0.02	100	0.97 ± 0.05
O_2^+	2.0	600	1.50 ± 0.12	0.036 ± 0.001	300	1.50 ± 0.12	250	2.20 ± 0.13
	1.0	250	0.46 ± 0.02	0.026 ± 0.003	300	0.46 ± 0.02	250	0.66 ± 0.03
Cs^+	2.0	150	0.82 ± 0.03	0.079 ± 0.005	200	1.90 ± 0.11	150	3.30 ± 0.18
	1.0	75	0.24 ± 0.01	0.046 ± 0.001	200	0.54 ± 0.03	150	0.96 ± 0.05

(Table 1). However, because the focus of 20 keV Ar_n^+ ion beam is better than either the Cs^+ beam or O_2^+ beam, a smaller sputter area is required for the same size analysis area when the Ar_n^+ source is used, which allows a higher sputter rate achieved in comparison with either the Cs^+ beam or O_2^+ beam (Figure S1 in the Supplemental Information).

For dual beam depth profiling, the sputter area needs to be considerably larger than the analysis area to avoid "crater edge" effect, and differs from one sputtering source to another for the same analysis area. We perform depth profiling of the $LaSrCrO_3/SrTiO_3$ sample (Supplementary Figure S2) using different sputtering sources at the same size of analysis area (100 × 100 μm²). The depth resolution, which can be defined as the depth interval over which the signal intensity of a selected ion varies from 16% to 84% at the sharp interface, is an important parameter to characterize the quality of depth profiling, and used as reference to decide the sputter size of a sputtering source requested for a certain analysis area. Figure 1 shows the relationship between the depth resolution and the sputter size for the three ion sources. The results show that when the sputter size is equal to or larger than 150 × 150 μm², the depth resolution of 20 keV Ar_n^+ sputtering becomes stable. As a comparison, 200 × 200 μm² is required for the Cs^+ source, and 300 × 300 μm² is required for the O_2^+ source. It means that the minimum sputter sizes for a 100 × 100 μm² analysis area are 150 × 150, 200 × 200, and 300 × 300 μm² for the Ar_n^+, the Cs^+, and the O_2^+ sources, respectively. Accordingly, the sputter rate of the 20 keV Ar_n^+ beam can reach 2.9 nm/s, which is faster than those of the 2.0 keV O_2^+ beam (1.5 nm/s) and the 2.0 keV Cs^+ beam (~1.9 nm/s). When a 50 × 50 μm² analysis area is required, the performance improvement of the Ar_n^+ beam over the O_2^+ or Cs^+ beams is even more pronounced (Table 1).

Surface/Interface Charging

Surface charging is a major challenge to ToF-SIMS depth profiling of insulating materials. Accumulated charges at the sputtering interface can change the energy distribution of the

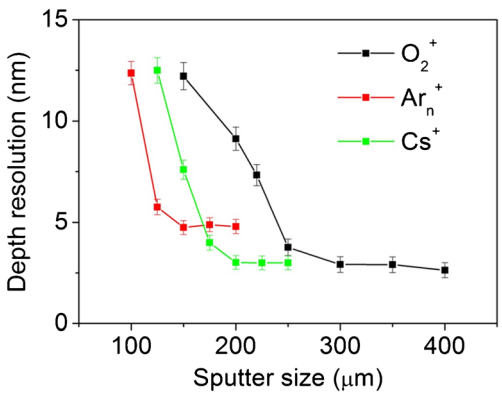

Figure 1. Depth resolution obtained at the interface of the $LaSrCrO_3/SrTiO_3$ film. A 100 μm × 100 μm analysis area (with 25 keV Bi^+ beam) was used, and the Cr^+ profile (Supplementary Figure S2 in the Supporting Materials) was chosen to calculate depth resolution

emitted secondary ions, degrading their transmission and detection by the mass spectrometer, which results in both low signal intensity and poor mass resolution. Despite the fact that a flood gun can be used for charge compensation, this does not work efficiently if a high sputter rate is needed because high sputter rates require both high sputter currents and an interlaced sputtering mode. Thus, insufficient charge compensation could be detrimental to the analysis of certain types of materials. For example, Li^+ diffusion in the SON68 glass during leaching can easily reach several μm deep. When a 2.0 keV O_2^+ sputtering beam was used to characterize Li^+ diffusion in the glass with interlaced mode, low $^7Li^+$ and $^6Li^+$ signals were observed. More seriously, a sudden anomalous drop of Li^+ signals was observed at a depth of ~2500 nm as shown in Figure 2. This is not an uncommon occurrence in glass depth profiling. Similar situations have been observed when using an O_2^+ beam in deep depth profiling of other glass materials, such as a glass microscope slide (data not shown here). Apparently, the accumulation of a larger amount of charges at the sputtering interface is responsive for the unreasonable experimental data. Though non-interlaced mode can solve this problem, the measurement time needs to be ~3 to 5 times longer.

Figure 3 and Table 2 show that signal intensity and mass resolution may improve if the energy and/or current of the sputtering beam is reduced, for example, changing the energy from 2.0 keV to 1.0 keV. But the sputter rates dramatically decrease as a consequence (Table 1), which in turn increase the measurement times as does the use of non-interlaced mode.

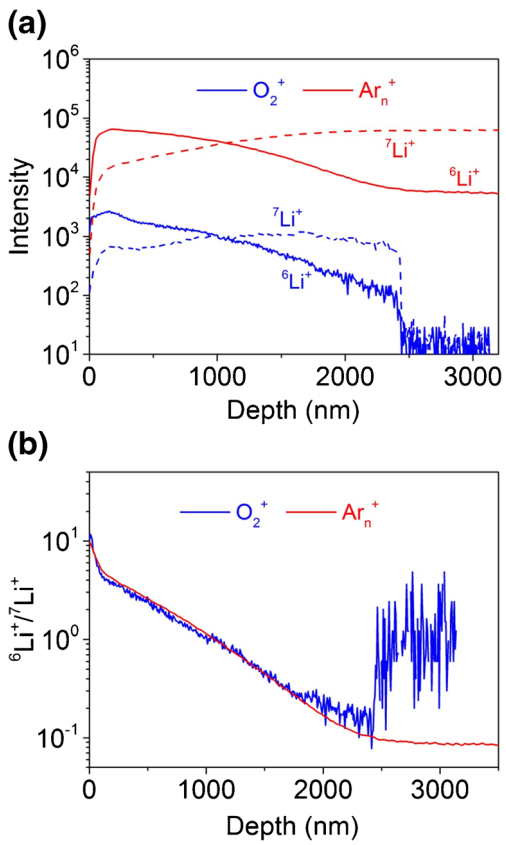

Figure 2. A comparison of interlaced mode depth profiles of ^7Li (dash line) and ^6Li (solid line) in a SON68 glass sample using 20 keV Ar_n^+(red) and 2 keV O_2^+ (blue) sputtering beams. (**a**) Intensity profiles; (**b**) ratio profiles

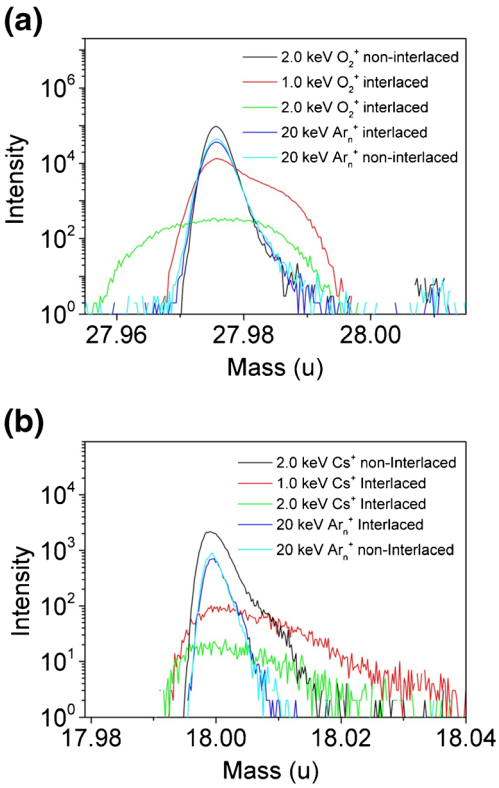

Figure 3. A comparison of (**a**) $^{28}Si^+$ and (**b**) $^{18}O^-$ peaks between different sputtering beams and modes on a SON68 glass sample. A 25 keV Bi^+ beam was used as analysis beam. For each spectrum, same setting of the analysis (Bi^+) beam (e.g., beam current, pulse width, pixel number, and frame number) was used

In a previous publication, we observed that a cluster ion sputtering source might reduce charging at the sputtering interface and enhance signal intensity of secondary ions [29]. In this study, when a 20 keV Ar_n^+ ion source was used for the SON68 glass sample, much stronger Li^+ signals were observed (Figure 2). The intensity of $^7Li^+$ and $^6Li^+$ was nearly 100 times higher than that observed by using the 2.0 keV O_2^+ source. In addition, no sudden drop of Li^+ signals (as well as the total ion signal, data not shown) occurred at ~2500 nm deep, even until 20 μm depth was reached.

It is worthy to note that using Ar_n^+ sputtering under interlaced mode provides not only high sputter rates and strong signal intensities but also good mass resolution. Figure 3 shows the $^{28}Si^+$ and $^{18}O^-$ peaks from the SON68 sample under different conditions of O_2^+, Cs^+, and Ar_n^+ sputtering. The mass resolution values are summarized in Table 2. The mass resolutions of the $^{28}Si^+$ peak from interlaced mode 2.0 and 1.0 keV O_2^+ sputtering are about 1600 and 5000, respectively, whereas the mass resolution from interlaced mode 20 keV Ar_n^+ sputtering is about 8200. Non-interlaced mode sputtering

Table 2. A Comparison of Mass Resolution and Signal Intensity of $^{28}Si^+$ and $^{18}O^-$ Peaks with Different Sputtering Beams and Sputtering Modes

Sputter ion and mode	$^{28}Si^+$ resolution	$^{28}Si^+$ area*	Sputter ion and mode	$^{18}O^-$ Resolution	$^{18}O^-$ area*
1 keV O_2^+ interlaced	4900	31%	1 keV Cs^+ interlaced	1300	15%
2 keV O_2^+ interlaced	1600	1.8%	2 keV Cs^+ interlaced	1000	3.5%
2 keV O_2^+ non-interlaced	9900	100%	2 keV Cs^+ non-interlaced	4600	100%
20 keV Ar_n^+ interlaced	8200	45%	20 keV Ar_n^+ interlaced	6000	25%
20 keV Ar_n^+ non-interlaced	8600	52%	20 keV Ar_n^+ non-interlaced	6600	28%

*This is a relative area. The $^{28}Si^+$ peak area from 2 keV O_2^+ sputtering with non-interlaced mode and the $^{18}O^-$ peak area from 2 keV Cs^+ sputtering with non-interlaced mode are set as references (100%)

provides the best mass resolution, ~9900 for 2.0 keV O_2^+ and ~8600 for 20 keV Ar_n^+, which can be attributed to an effective charge compensation. A more interesting observation is that the mass resolution of $^{18}O^-$ from Ar_n^+ sputtering is better than that from non-interlaced Cs^+ sputtering. A plausible explanation is that Cs implantation changes the electric properties of the sputtering interface, whereas Ar_n^+ sputtering does not result in this effect. This virtue is very valuable in glass corrosion research. As mentioned earlier, isotopically enriched glass samples have been introduced to elucidate the corrosion mechanisms of glass, and SIMS has been a major technique to characterize isotopic depth profiles in these samples [27]. However, mass interferences have been a problem for interlaced mode O_2^+ depth profiling. For example, for the ToF-SIMS analysis of ^{44}Ca and ^{57}Fe enriched SON68 glass samples, an interference peak, $^{28}Si^{16}O^+$ (m/z = 43.972), is very close to $^{44}Ca^+$ (m/z = 43.956), and a minimum mass resolution of 2700 is required to separate the pair of ions. Similarly, $^{40}Ca^{16}O^+$ (m/z = 55.958) is very close to $^{56}Fe^+$ (m/z = 55.935), and a minimum mass resolution of 2500 is required to distinguish them. In practice, at least twice the minimum mass resolution is required to obtain reasonable measurement precision. The traditional solution to obtain decent mass resolution in depth profiling of insulator samples is to use the non-interlaced mode, but the cost in time may not be affordable for many applications.

We already show that with the use of an Ar_n^+ sputtering beam, high sputter rates, high mass resolution (>8000), and reasonable signal intensities can be obtained simultaneously. Compared with O_2^+ or Cs^+ sputtering, depth profiling of glass samples using an Ar_n^+ sputtering source can dramatically reduce experimental time (9- to 15-fold time-saving) without compromise of data quality. The 9- to 15-fold time-saving is estimated because both interlaced mode and smaller sputter area can be used for "high-speed" Ar_n^+ sputtering, but none of them is practical for traditional "high-speed" O_2^+ or Cs^+ sputtering. This advantage is especially important for deep depth profiling (e.g., ≥3 μm) because the measurement time is very long if Cs^+ or O_2^+ sputtering is used.

In Table 2, the signal intensity and mass resolution of the $^{28}Si^+$ or $^{18}O^-$ peak with non-interlaced mode 20 keV Ar_n^+ sputtering is only slightly (5%–15%) better than that from interlaced mode. This means that with interlaced mode 20 keV Ar_n^+ sputtering, the charge compensation is very effective, though it may not be as good as that with non-interlaced mode. As a comparison, interlaced and non-interlaced mode using 2.0 keV O_2^+ sputtering show ~6 times difference in mass resolution and ~560 times difference in signal intensity for the $^{28}Si^+$ signal. Interlaced and non-interlaced mode using 2.0 keV Cs^+ sputtering show ~7 times difference in mass resolution and ~30 times difference in signal intensity for the $^{18}O^-$ signal. Apparently, Ar_n^+ sputtering leads to much lower charge residuals at the sputtering interface, which may be attributed to two reasons. First, as shown in Table 2, the sputtering yield of a 20 keV Ar_n^+ ion is about 0.88 nm^3/ion, much larger than that of a 2.0 keV Cs^+ ion (0.079 nm^3/ion) or an O_2^+ ion (0.036 nm^3/ion). Therefore, the implanted charge number with Ar_n^+ sputtering is much lower. At the same time, a big Ar_n^+ cluster (e.g., n = 1500 for the 20 keV Ar_n^+ used in this work) would break down to many single Ar atoms and small Ar clusters at the sputtering interface. These Ar atoms and small Ar clusters can take some charges away from the sputtering interface. The advantages of Ar_n^+ sputtering over traditional O_2^+ and Cs^+ sputtering in depth profiling of insulator samples have been schematically illustrated in Figure 4.

The advantage that the Ar_n^+ sputtering can provide a low charging sputtering interface during interlaced mode depth profiling of insulating samples was verified further by analyzing the multilayer functional thin oxide films on insulating substrate. This sample was prepared by growing a 50 nm $SrCrO_3$ thin film and then a 50 nm $SrTiO_3$ thin film on $SrTiO_3$ substrate ($SrTiO_3$/$SrCrO_3$/$SrTiO_3$) in $^{18}O_2$ atmosphere, and ^{18}O is found to be diffused into the $SrTiO_3$ substrate with a significant depth (~10 μm as shown in Figure 5a). An Ar_n^+ sputtering beam (20 keV) with interlaced mode was used to measure ^{18}O diffusion behavior. It took about 4 h (sputter rate was about 1.1 nm/s, 10.0 nA Ar_n^+ beam, 200 × 200 μm^2 sputter area) to perform this measurement. The results show that the ^{18}O diffuses into the $SrTiO_3$ substrate for about 12 μm. As a comparison, if a 2.0 keV Cs^+ sputtering source is used with interlaced mode, the sputter rate is about 0.31 nm/s (100 nA Cs^+ beam, 300 × 300 μm^2 sputter area). The $^{18}O^-/(^{18}O^- + {}^{16}O^-)$ depth profile with Cs^+ sputtering is shown in Figure 5b. It was surprising to observe that in a range from the $SrTiO_3$/$SrCrO_3$ interface (~50 nm deep) to a depth of ~400 nm, the Cs^+ data is significantly higher and noisier than the Ar_n^+ data. To validate the data reliability, we reduced the Ar_n^+ beam current, to make its sputter rate similar to the Cs^+ source sputter rate, and the data from this measurement match well with the data from the

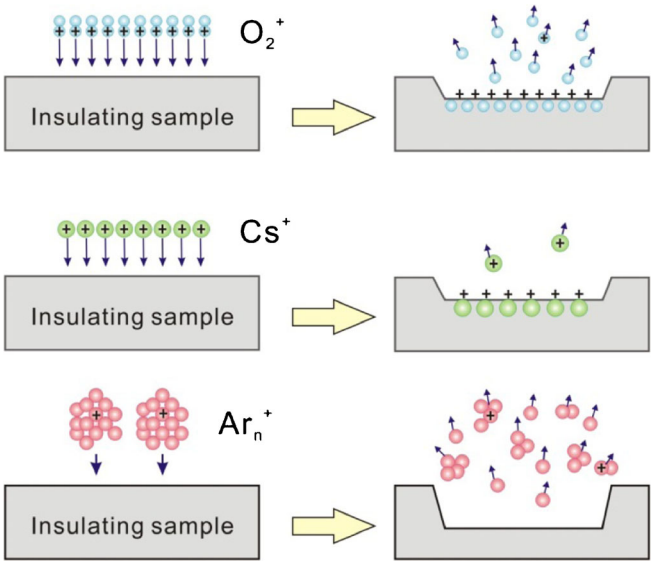

Figure 4. A schematic illustration of the advantage of Ar_n^+ sputtering over O_2^+ and Cs^+ sputtering in depth profiling of insulating samples. Although implantation of O and Cs atoms may improve ionization yield, O_2^+ and Cs^+ sputtering introduces too many residual charges at the sputtering interface on insulating samples. As a comparison, a low charging sputtering interface can be obtained with Ar_n^+ sputtering because (1) the high sputter yield per Ar_n^+ ion leads to much less charges implanted in to the sputtering interface; and (2) a big Ar_n^+ ion would break into many single Ar atoms and small Ar clusters, which can take some charge away from the sputtering interface

high-current Ar_n^+ sputtering data. In addition, non-interlaced mode depth profiling using the Cs^+ sputtering source shows a result similar to the Ar_n^+ data (Figure 5b). These results suggest that there was a problem with interlaced mode depth profiling using the 2.0 keV Cs^+ beam. After carefully checking the O^- signal intensity and peak shape, we found that the total O^- signal ($^{18}O^- + {}^{16}O^-$) with 2.0 keV Cs^+ interlaced mode had a big drop from ~50 nm to ~100 nm (in the $SrCrO_3$ layer). The total O^- signal showed a jump at the $SrCrO_3$/substrate interface (~100 nm deep) and gradually increases until ~400 nm, where the intensity of the total O^- signal is similar to that from the surface $SrTiO_3$ layer (0–50 nm) (Figure 5c). At the same time, the O^- peak centers shift in this depth range (data are not shown here). The signal drop and peak shift can be attributed to the different electrical conductivity in the different layers, which leads to a dramatic and continuous change in the charging state during the interlaced Cs^+ sputtering. The non-interlaced mode can be used to avoid this pitfall (Figure 5c), but the cost in time may be an issue. As a comparison, interlaced mode Ar_n^+ sputtering data show limited signal intensity variations and peak shifting. These imply that erroneous results may manifest themselves because of a variable charging state with interlaced mode Cs^+ depth profiling, whereas Ar_n^+ sputtering beam can be used with interlaced mode without serious charging effect, providing accurate chemical information in the interface of multilayer oxide films on insulating substrate.

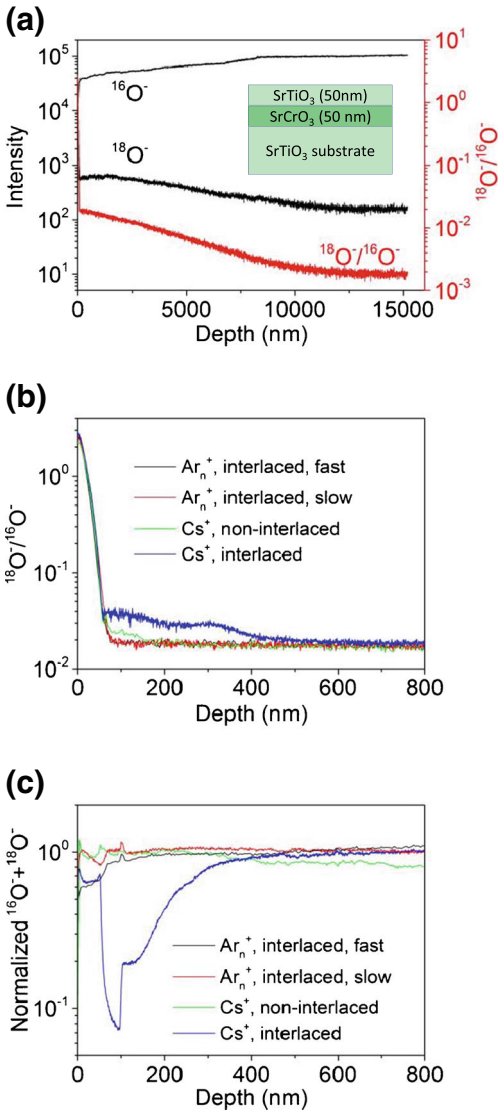

Figure 5. $^{16}O^-$ and $^{18}O^-$ depth profiles in a $SrTiO_3/SrCrO_3$ thin film sample on $SrTiO_3$ substrate. (**a**) 20 keV 12 nA Ar_n^+ sputtering beam under interlaced mode. (**b**) $^{18}O^-/(^{16}O^- + {}^{18}O^-)$ depth profiles using different sputtering sources and sputtering modes. (**c**) Depth profiles of normalized oxygen signal ($^{16}O^- + {}^{18}O^-$) with different sputtering sources and sputtering modes

Ionization Yield

Compared with traditional O_2^+ and Cs^+ sputtering sources, a major concern with the use of Ar_n^+ sputtering in inorganic depth profiling is the lack of the capability to enhance ionization yield. For example, the Si^+ and Si^- signals are weak if an Ar_n^+ sputtering beam is used to perform depth profiling of a silicon wafer. Our data show that compared with 20 keV Ar_n^+ sputtering, 2.0 keV Cs^+ sputtering can provide ~2000 times signal enhancement for Si^-, and 2.0 keV O_2^+ sputtering can provide ~50 times signal enhancement for Si^+ on a silicon wafer. However, ionization yield enhancement may not be a problem for glasses or other oxide samples because these materials are generally ionic structures, guaranteeing

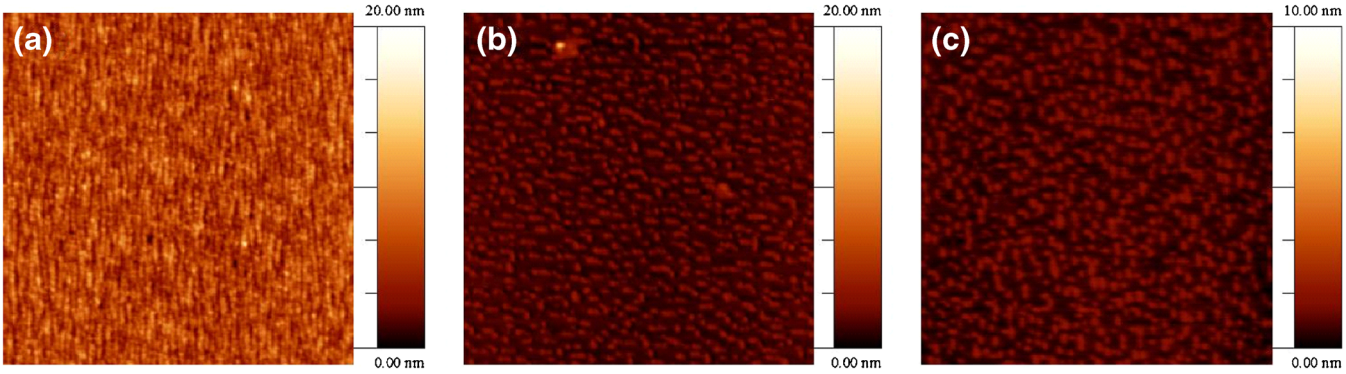

Figure 6. AFM images at the crater center areas on the 66 nm thick $LaSrCrO_3$ film on $SrTiO_3$ substrate after sputtering with (**a**) 20 keVAr_n^+, (**b**) 2.0 keV O_2^+, (**c**) 2.0 keV Cs^+ beams. All crater depth is about 100 nm

reasonable ionization yields with any sputtering source. To compare the ionization yield difference, non-interlaced mode depth profiling with O_2^+, Cs^+, and Ar_n^+ sputtering was performed on the SON68 glass sample. The $^{28}Si^+$ and $^{18}O^-$ peaks were used as representative signals (Figure 3 and Table 2). If defining the $^{28}Si^+$ peak area from 2.0 keV O_2^+ non-interlaced mode sputtering was 100%, the relative peak area of the $^{28}Si^+$ arising from 20 keV Ar_n^+ non-interlaced mode sputtering was ~50%. This indicates that for this glass sample, the ionization yield enhancement using O_2^+ sputtering is only twice that using 20 keV Ar_n^+ sputtering, which is much smaller than the enhancement value (~50 times) of Si^+ on a silicon wafer. Similarly, Cs^+ sputtering provides only a mild ionization yield enhancement (~3 times) compared with Ar_n^+ sputtering, and is also much smaller than that (~2000 times) for Si^- signal on a silicon wafer. Similar results have been observed on other glass and oxide samples (data not shown here).

Roughness of Sputtering Interface

As we discussed above, the high sputtering yield of a 20 keV Ar_n^+ ion leads to a low charging sputtering interface, allowing us to perform fast depth profiling of glass and functional oxide samples with very limited sacrifice of signal intensity and mass resolution. However, there are still some issues related to the use of this sputtering source. For example, it may increase the roughness of the sputtering interface if one compares the interface to that obtained with O_2^+ and Cs^+ sources. Figure 6 shows the AFM images in the crater bottom on the $LaSrCrO_3/SrTiO_3$ thin film sample after sputtering with 20 keV Ar_n^+, 2.0 keV O_2^+, and 2.0 keV Cs^+ beam, respectively. The RMS (root mean square) roughness of the Ar_n^+ crater bottom is about 9–10 nm, the comparable RMS values of the O_2^+ and the Cs^+ craters are about 4–5 and 3–4 nm, respectively. These results correspond to the data shown in Figure 1, where the best depth resolution of the 20 keV Ar_n^+ sputtering at the $LaSrCrO_3/SrTiO_3$ interface is about 5 nm, approximately two times that of the 2.0 keV Cs^+ or the 2.0 keV O_2^+ sputtering (2–3 nm). These results are not in agreement with the general concept that cluster sputtering ions provide a much smoother sputtering interface than single atom sputtering ions used with similar energy [30]. However, we noticed that previous reports in the literature normally compared the roughness induced by various sputtering sources used with similar energy, where the roughness induced by single atom ions is much worse than cluster ions. If the energy used to different sputtering sources is largely different, the situation may become complicated because the roughness induced by a sputtering ion may increase with increase in the used energy. For example, focused ion beam and atom probe tomography (FIB-APT) experiments showed that 30 keV Ga^+ ion beam can cause damage in a Si sample as deep as 40 nm, but the damage layer induced by 2 keV Ga^+ is less than 1 nm thick [31]. Taking this into account, the poor roughness induced by Ar cluster sputtering sources observed in the present work may be attributed to the high energy (20 keV) used during the sputtering; the comparable energy used during the Cs^+ or O_2^+ sputtering was 2.0 keV.

Conclusions

We have demonstrated the superior performance of an Ar_n^+ sputtering source relative to traditional O_2^+ and Cs^+ sputtering sources for depth profiling of various inorganic insulating samples in terms of their sputter rates and accuracy of interfacial chemical information. Because of the high sputter rate and low charge accumulation of the Ar_n^+ sputtering source, interlaced mode of dual-beam depth profiling can be easily performed on insulating samples without compromising the depth and interfacial chemical information. Although Ar_n^+ sputtering sources may cause some roughness problem, the measurement time of depth profiling of an insulating sample using an Ar_n^+ sputtering source can be dramatically reduced compared with traditional O_2^+ and Cs^+ sputtering sources, making it a feasible sputtering source for magnetic SIMS, XPS, and other depth profiling besides ToF-SIMS. The implementation of an Ar_n^+ sputtering source can enhance the capabilities for analysis of insulating materials and, thus, expand applications in the field of glass corrosion, study of functional thin films on insulating substrates, and many other potential fields related to insulating materials with complex layered structures.

Acknowledgments

F.Y.W and Z.Y.W thank the NSFC (grant no. 21127901, 21135006, 21321003) for support. This work was partially funded by the U.S. Department of Energy Office of Nuclear Energy (Fuel Cycle Research and Development) and Office of Environmental Management (Tank Waste Managementt, EM-21). The work was performed at EMSL, a national scientific user facility sponsored by the Department of Energy's Office of Biological and Environmental Research located at PNNL.

References

1. Vickerman, J.C., Briggs, D.: Tof-Sims: Materials Anaylysis by Mass Spectrometry. ToF-SIMS Materials Analysis by Mass Spectrometry, p. 753. IM Publications and SurfaceSpectra Ltd, Chichester (2001)
2. Vickerman, J.C., Briggs, D.: ToF-SIMS Materials Analysis by Mass Spectrometry, 2nd edn, pp. 553–709. IM Publications and SurfaceSpectra Ltd, Chichester (2013)
3. Anderson, O., Scheumann, V., Rothhaar, U., Rupertus, V.: Surface and depth profile analysis of insulating samples by ToF-SIMS. Glass Sci. Technol. **77**, 159–165 (2004)
4. Toyoda, N., Matsuo, J., Aoki, T., Yamada, I., Fenner, D.B.: Secondary ion mass spectrometry with gas cluster ion beams. Nucl. Instrum. Methods B **190**, 860–864 (2002)
5. Toyoda, N., Matsuo, J., Aoki, T., Yamada, I., Fenner, D.B.: Secondary ion mass spectrometry with gas cluster ion beams. Appl. Surf. Sci. **203**, 214–218 (2003)
6. Miyayama, T., Sanada, N., Bryan, S.R., Hammond, J.S., Suzuki, M.: Removal of Ar+ beam-induced damaged layers from polyimide surfaces with argon gas cluster ion beams. Surf. Interface Anal. **42**, 1453–1457 (2010)
7. Yun, D.J., Chung, J., Kim, S.H., Kim, Y., Seol, M., Chung, J., Park, S.H.: Study on the molecular distribution of organic composite films by combining photoemission spectroscopy with argon gas cluster ion beam sputtering. J. Mater. Chem. C **3**, 276–282 (2015)
8. Ninomiya, S., Ichiki, K., Yamada, H., Nakata, Y., Seki, T., Aoki, T., Matsuo, J.: Molecular depth profiling of multilayer structures of organic semiconductor materials by secondary ion mass spectrometry with large argon cluster ion beams. Rapid Commun. Mass Spectrom. **23**, 3264–3268 (2009)
9. Lee, J.L.S., Ninomiya, S., Matsuo, J., Gilmore, I.S., Seah, M.P., Shard, A.G.: Organic depth profiling of a nanostructured delta layer reference material using large argon cluster ions. Anal. Chem. **82**, 98–105 (2010)
10. Rabbani, S., Barber, A.M., Fletcher, J.S., Lockyer, N.P., Vickerman, J.C.: ToF-SIMS with argon gas cluster ion beams: a comparison with C-60(+). Anal. Chem. **83**, 3793–3800 (2011)
11. Shard, A.G., Havelund, R., Seah, M.P., Spencer, S.J., Gilmore, I.S., Winograd, N., Mao, D., Miyayama, T., Niehuis, E., Rading, D., Moellers, R.: Argon cluster ion beams for organic depth profiling: results from a VAMAS Interlaboratory Study. Anal. Chem. **84**, 7865–7873 (2012)
12. Fletcher, J.S., Vickerman, J.C.: Secondary Ion mass spectrometry: characterizing complex samples in two and three dimensions. Anal. Chem. **85**, 610–639 (2013)
13. Bich, C., Havelund, R., Moellers, R., Touboul, D., Kollmer, F., Niehuis, E., Gilmore, I.S., Brunelle, A.: Argon cluster ion source evaluation on lipid standards and rat brain tissue samples. Anal. Chem. **85**, 7745–7752 (2013)
14. Liao, H.Y., Tsai, M.H., Kao, W.L., Kuo, D.Y., Shyue, J.J.: Effects of the temperature and beam parameters on depth profiles in x-ray photoelectron spectrometry and secondary ion mass spectrometry under C-60(+)-Ar+ cosputtering. Anal. Chim. Acta **852**, 129–136 (2014)
15. Cumpson, P.J., Portoles, J.F., Sano, N.: Observations on X-ray enhanced sputter rates in argon cluster ion sputter depth profiling of polymers. Surf. Interface Anal. **45**, 601–604 (2013)
16. Lu, P., Fu, Q., Seyfried, W.E., Hedges, S.W., Soong, Y., Jones, K., Zhu, C.: Coupled alkali feldspar dissolution and secondary mineral precipitation in batch systems-2: new experiments with supercritical Co_2 and implications for carbon sequestration. Appl. Geochem. **30**, 75–90 (2013)
17. Brantley, S.L., Kubicki, J.D., White, A.F.E.: Kinetics of Water-Rock Interaction, pp. 2151–2210. Springer, New York (2008)
18. McGrail, B.P., Icenhower, J.P., Shuh, D.K., Liu, P., Darab, J.G., Baer, D.R., Thevuthasen, S., Shutthanandan, V., Engelhard, M.H., Booth, C.H., Nachimuthu, P.: The structure of Na_2O-Al_2O_3-SiO_2 glass: impact on sodium ion exchange in H_2O and D_2O. J. Non-Cryst. Solids **296**, 10–26 (2001)
19. Ferrand, K., Abdelouas, A., Grambow, B.: Water diffusion in the simulated French nuclear waste glass son 68 contacting silica rich solutions: experimental and modeling. J. Nucl. Mater. **355**, 54–67 (2006)
20. Neeway, J., Abdelouas, A., Grambow, B., Schumacher, S.: Dissolution Mechanism of the SON68 Reference Nuclear Waste Glass: New Data in Dynamic System in Silica Saturation Conditions. J. Nucl. Mater. **415**, 31–37 (2011)
21. Cailleteau, C., Angeli, F., Devreux, F., Gin, S., Jestin, J., Jollivet, P., Spalla, O.: Insight into silicate-glass corrosion mechanisms. Nat. Mater. **7**, 978–983 (2008)
22. Jollivet, P., Angeli, F., Cailleteau, C., Devreux, F., Frugier, P., Gin, S.: Investigation of gel porosity clogging during glass leaching. J. Non-Cryst. Solids **354**, 4952–4958 (2008)
23. Valle, N., Verney-Carron, A., Sterpenich, J., Libourel, G., Deloule, E., Jollivet, P.: Elemental and isotopic (Si-29 and O-18) tracing of glass alteration mechanisms. Geochim. Cosmochim. Acta **74**, 3412–3431 (2010)
24. Chambers, S.A., Engelhard, M.H., Shutthanandan, V., Zhu, Z., Droubay, T.C., Qiao, L., Sushko, P.V., Feng, T., Lee, H.D., Gustafsson, T., Garfunkel, E., Shah, A.B..., Zuo, J.M., Ramasse, Q.M.: Instability, intermixing and electronic structure at the epitaxial $LaAlO_3/SrTiO_3(001)$ heterojunction. Surf. Sci. Rep. **65**, 317–352 (2010)
25. Schlom, D.G., Chen, L.Q., Pan, X.Q., Schmehl, A., Zurbuchen, M.A.: A Thin film approach to engineering functionality into oxides. J. Am. Ceram. Soc. **91**, 2429–2454 (2008)
26. Zhang, K.H.L., Sushko, P.V., Colby, R., Du, Y., Bowden, M.E., Chambers, S.A.: Reversible nano-structuring of $SrCrO_3$-δ through oxidation and reduction at low temperature. Nat. Commun. **5**, 4669 (2014)
27. Neeway, J., Sebastien, K.G.S., Wang, Z., Zhu, Z., Ryan, J.: Low-temperature lithium diffusion in simulated high-level boroaluminosilicate nuclear waste glasses. J. Non-Cryst. Solids **405**, 83–90 (2014)
28. Wang, Z., Jin, K., Zhang, Y., Wang, F., Zhu, Z.: Tof-SIMS depth profiling of insulating samples, interlaced mode or non-interlaced mode? Surf. Interface Anal. **46**, 257–260 (2014)
29. Zhu, Z.H., Shutthanandan, V., Nachimuthu, P.: Using C-60(+) Sputtering to improve detection limit of nitrogen in zinc oxide. Surf. Interface Anal. **43**, 661–663 (2011)
30. Sun, S., Wucher, A., Szakal, C., Winograd, N.: Depth profiling of polycrystalline multilayers using a buckminsterfullerene projectile. Appl. Phys. Lett. **84**, 5177–5179 (2004)
31. Thompson, K., Lawrence, D., Larson, D.J., Olson, J.D., Kelly, T.F., Gorman, B.: In situ site-specific specimen preparation for atom probe tomography. Ultramicroscopy **107**, 131–139 (2007)